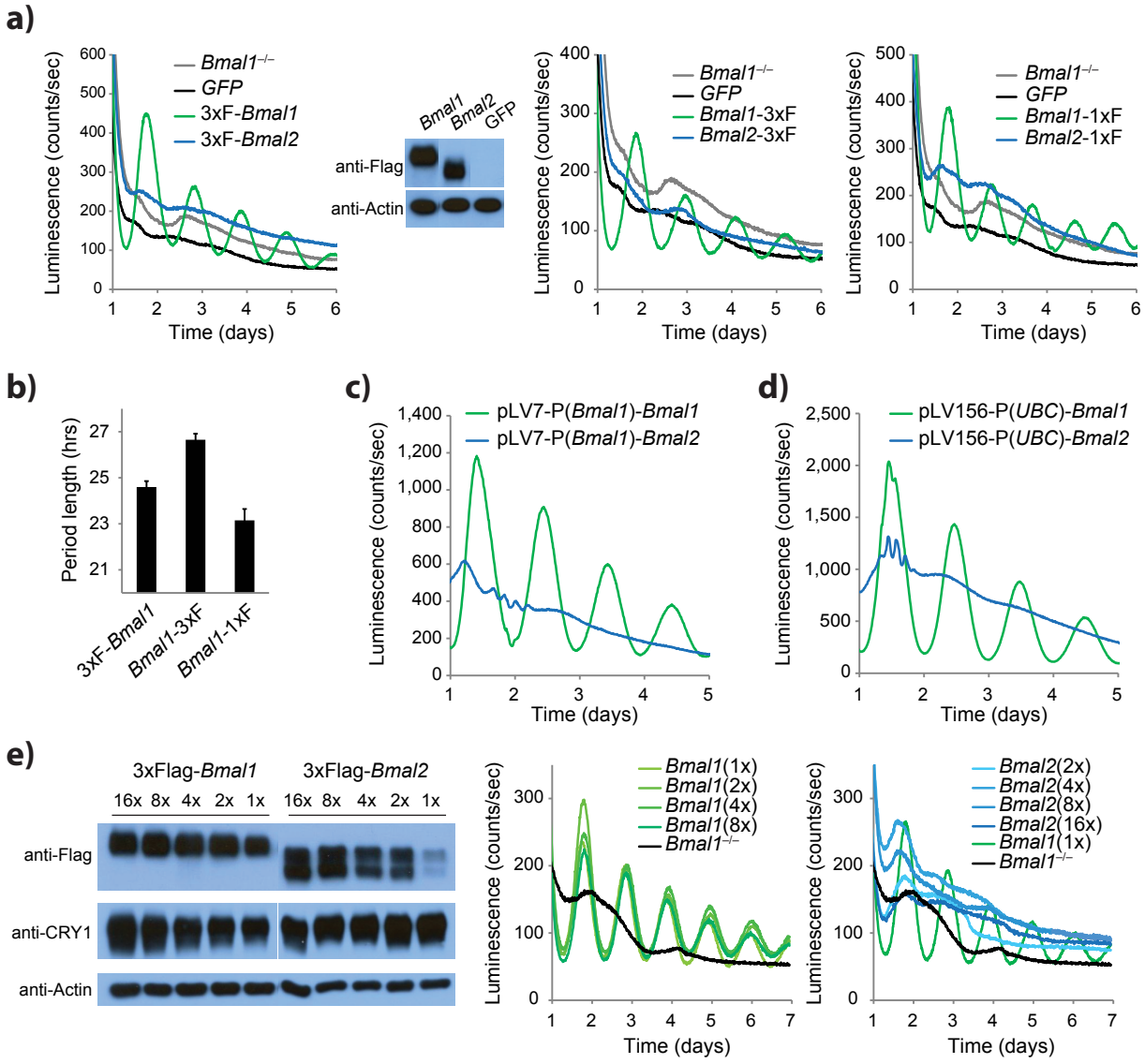

Supplementary Figure 1. Validation of genetic complementation assay in *Bmal1*$^{-/-}$ *Per2*^{Luc} fibroblasts. **(a)** Only *Bmal1*, not *Bmal2*, rescues circadian rhythms from cells. Cells expressing various *Bmal* constructs (Flag-tagged at either the N- or- C-terminus) were subjected to cycling analysis: 3xF-*Bmal*, *Bmal* tagged with 3xFlag at the N-terminus; *Bmal*-3xF, 3xFlag tag at the C-terminus; *Bmal*-1xF, 1xFlag at the C-terminus. A representative western blot of 3xF-BMAL proteins (inset) shows that *Bmal1* and *Bmal2* were expressed to similar levels off the plasmid. **(b)** Period length analysis of rescued rhythms in panel (**a**). Data are plotted as mean ± s.d. error bars from 3 independent clonal lines. Placement of Flag tags seems to impact period length. For this consideration, we tested both 3xF-Bmal and Bmal1-1xF constructs throughout the study and similar results from domain swaps/mutants were obtained. **(c)** Cyclic expression of *Bmal1*, but not *Bmal2*, rescues circadian rhythms in *Bmal1*$^{-/-}$ *Per2*^{Luc} fibroblasts. A fragment of the *Bmal1* promoter that contains circadian RORE cis-elements was used to drive *Bmal* transcription. Expression of *Bmal2* under control of the rhythmic *Bmal1* promoter was unable to rescue rhythms. For consistency, the *UBC* promoter was used throughout this study. (**d)** The ability of *Bmal1* to rescue rhythms does not depend on the expression vector used. The pLV156 vector expresses an IRES-mediated GFP while the recombination-based pLV7 vector confers high efficiency cloning. Expression of *Bmal1* off the pLV7 plasmid reconstituted cycling and was therefore used throughout this study. (**e)** The ability of *Bmal1* to rescue rhythms is dosage independent. Protein expression levels at various levels of infection were determined by Western blot (left panel). While *Bmal1* rescued circadian rhythms under all expression regimes tested (center panel), *Bmal2* failed to rescue levels even at high levels of expression (right panel). We note that CRY1 displayed a modest dose response to the titration of BMAL1 levels, but demonstrated no effect upon BMAL2 titration.

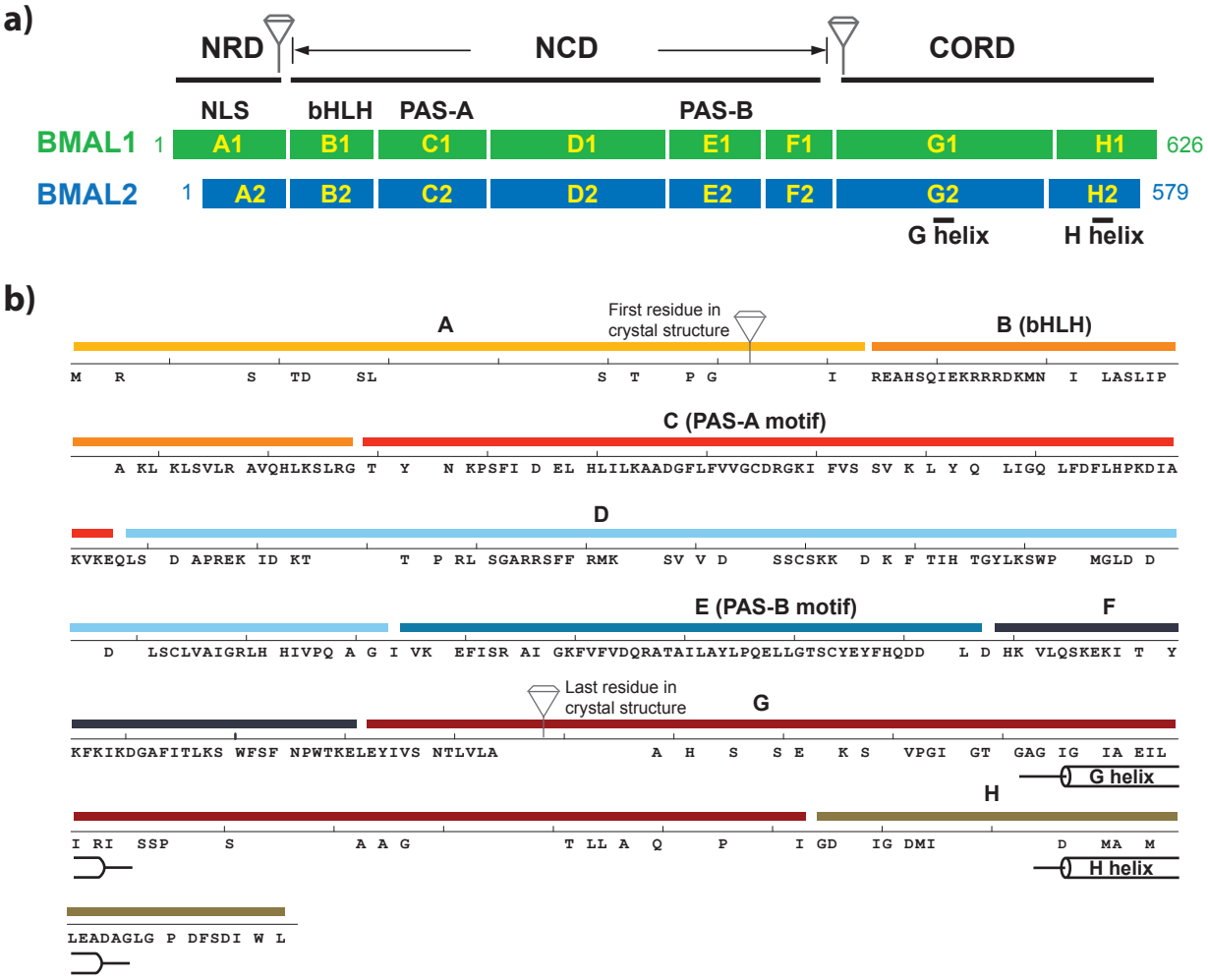

Supplementary Figure 2. Domain structure, sequence alignment and structural features of BMAL1 and BMAL2. (**a)** Schematic diagram of domain structure of BMAL1 (green) and BMAL2 (blue); cartoons drawn to scale. NRD, N-terminal regulatory domain; NCD, N-terminal core domain; CORD, C-terminal oscillator regulatory domain. The BMAL1-NRD (region A) contains a nuclear localization signal (NLS) that is not conserved in BMAL2. The NCD contains the bHLH DNA-binding domain (region B), PAS-A motif (region C), and PAS-B motif (E). The CORD contains regions G and H. Diamonds indicate boundaries for the protein fragment for which a crystal structure is available (PDB 4F3L)[14]. Each motif color corresponds to the circadian bioluminescence data for complemented *Bmal1*$^{-/-}$ *Per2*^{Luc} fibroblasts in Figure 2b and 2e. (**b)** Sequence alignment of BMAL1 and BMAL2 demonstrates divergence of CORD sequences. Mouse BMAL protein sequences were aligned in Vector NTI. Consensus sequence is shown in black. White barrels indicate JPred-predicted secondary structure (α-helices) in the CORD.

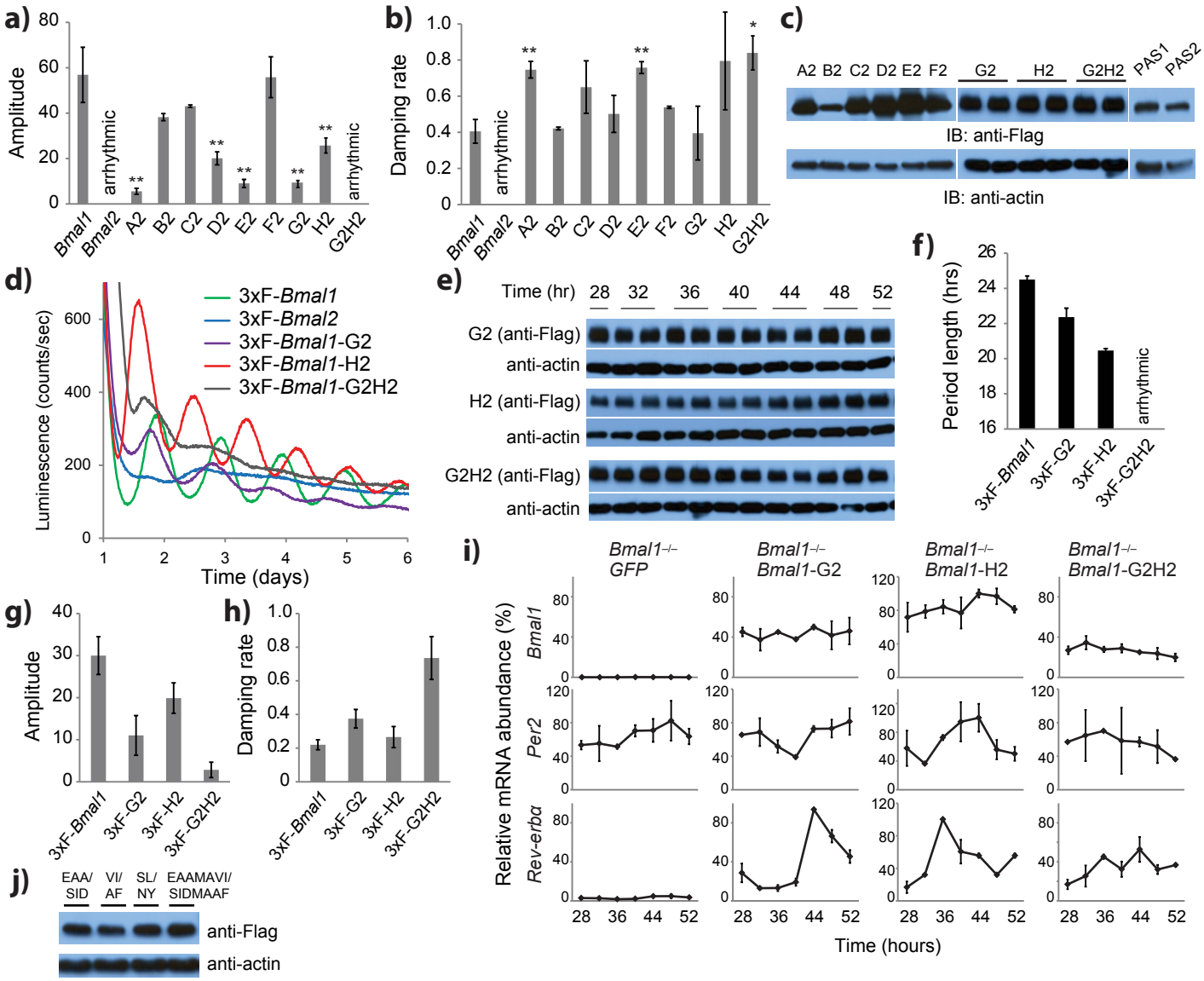

Supplementary Figure 3. The C-terminal regulatory domain of BMAL1 is critical for maintaining circadian period length and rhythm amplitude. (**a-c)** Analysis of **(a)** amplitude and **(b)** damping rates and **(c)** expression of *Bmal1*, *Bmal2*, and chimeric *Bmal1-Bmal2* constructs from Figure 2. Data are plotted as mean ± s.d. error bars from 3 independent clonal lines. Relative protein expression levels were determined by western blot using indicated antibodies. (**d)** Both G and H regions of the BMAL1 C-terminus are required to reconstitute circadian cycling in *Bmal1*$^{-/-}$ *Per2*^{Luc} fibroblasts. Experimental details are the same as in Figure 2, except that 3xFlag-*Bmal* constructs were used here (while *Bmal*-1xF constructs were used throughout the main figures of the paper). (**e)** Relative expression levels of mutant chimeric proteins were determined by western blot over a time course after synchronization of clocks by dexamethasone treatment (time = 0). Expression of BMAL1-G2, H2, or G2H2 chimeric proteins was determined using Flag antibody; actin is shown as a loading control. (**f-h)** Analysis of **(f)** period length, **(g)** amplitude, **(h)** and damping rates for 3xF-*Bmal* constructs shown in panel **(d)**. Data are plotted as mean ± s.d. error bars from 3 independent clonal lines. (**i)** Temporal expression profiles of clock gene mRNA in *Bmal1*$^{-/-}$ *Per2*^{Luc} fibroblasts expressing *Bmal1*-G2, H2, or G2H2. Values are expressed as percentage of maximum expression for each gene from 3 independent assays and can be directly compared with those in Figure 1c. Data are plotted as mean ± s.d. of expression levels from two independent cell culture samples (including triplicate technical replicates) for each cell line. Time, hours after dexamethasone synchronization. **(j)** Western blot analysis of mutant BMAL1 expression in 293T cells detected by Flag antibody. Similar results were obtained from *Bmal1*$^{-/-}$ *Per2*^{Luc} fibroblasts expressing various forms of the mutant BMAL1 proteins corresponding to cell lines shown in Figure 3 (data not shown). * $P < 0.05$; ** $P < 0.01$ compared to *Bmal1* by two-tailed paired t test.

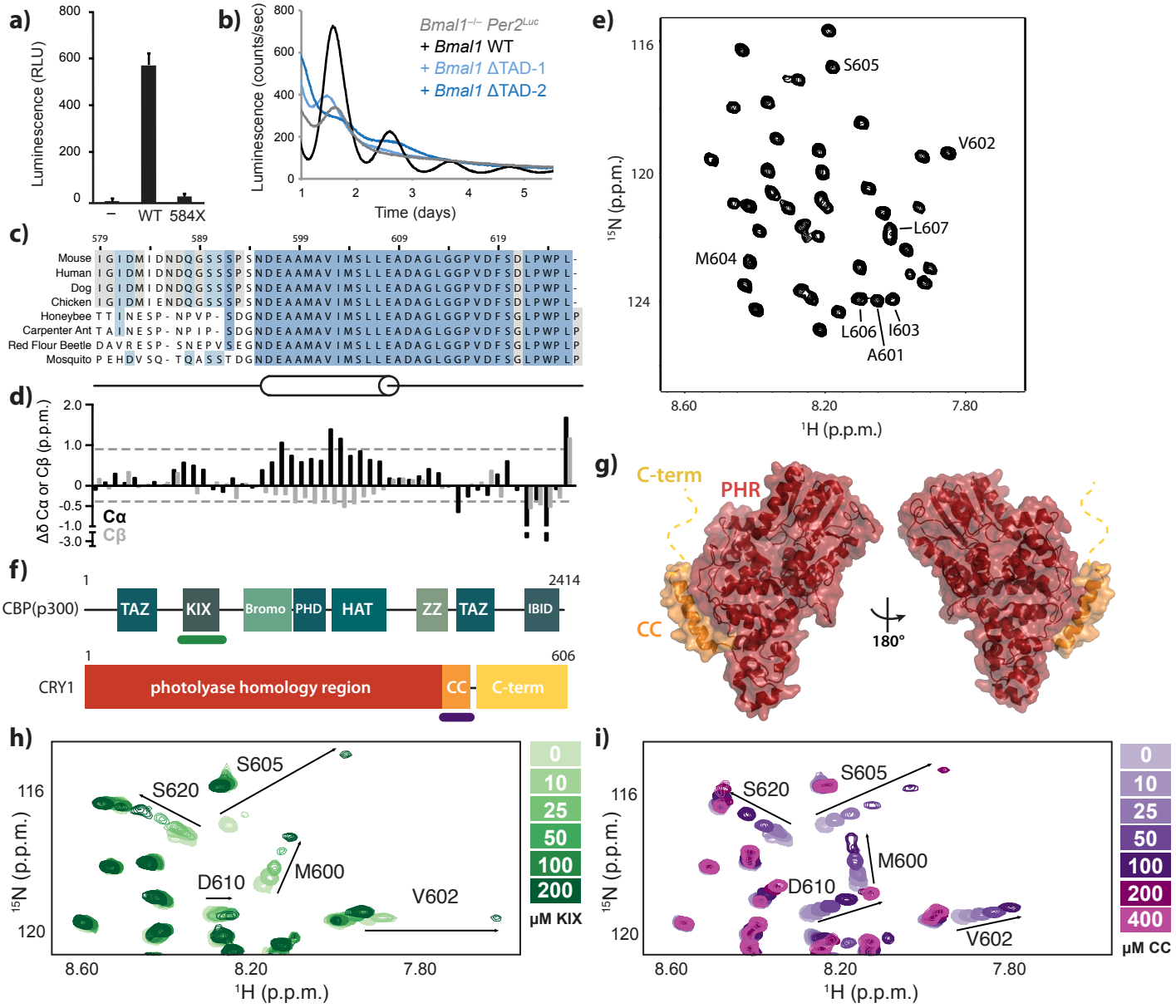

Supplementary Figure 4. The BMAL1 TAD interacts directly with transcriptional coregulators and is required for CLOCK–BMAL1 activity. **(a)** Deletion of the BMAL1 TAD by truncation at residue 584 (584X) eliminates CLOCK–BMAL1 activation of a *Per1*-luciferase reporter gene in HEK293T cells. Data are plotted as mean relative luminescence counts (x 10^3) ± s.d. error bars for three independent replicates. **(b)** The BMAL1 TAD is required to generate circadian rhythms. Representative bioluminescence records from *Bmal1*$^{-/-}$ *Per2*^{Luc} fibroblasts complemented with the indicated *Bmal1* constructs (ΔTAD indicates truncation of H region). **(c)** Conservation of TAD primary sequence and secondary structure across metazoan species with a vertebrate-like clock[29]. Blue barrel, predicted α-helix (JPred); black line, no predicted structure. **(d)** The TAD has a modest propensity for α-helix formation, demonstrated by comparison of Cα (black) or Cβ (gray) chemical shifts to the chemical shift index of random coil shifts (Δδ)[31,32]. Residues correspond to alignment and secondary structure prediction in panel **(c)**. Dashed line: significance cutoff for helical prediction from Δδ. **(e)** Central region of the ^{15}N HSQC spectrum of the BMAL1 TAD displays the modest chemical shift dispersion typical of unfolded/partly helical proteins. Assignments for residues of the IxxLL motif in the α-helix are indicated. p.p.m., parts per million. **(f)** Modular domain architecture of CBP(p300) (green) and CRY1 (red), with domains used in the present study underlined. **(g)** Crystal structure of mouse CRY1 (PDB 4K0R)[23] displayed with domain coloring from panel **(f)**. The PHR domain comprises most of CRY1, followed by the CC helix (orange), which forms the final α-helix before the disordered C-terminus (yellow dashed line). **(h-i)** The CBP(p300) KIX domain and CRY1 CC helix bind overlapping regions on the BMAL1 TAD. A highlighted region of ^{15}N HSQC spectra from ^{15}N BMAL1 TAD titrated with increasing concentrations of either p300 KIX **(h)** or the monomeric CRY1 CC peptide **(i)** show perturbation of the same residues. CBP KIX induces the same perturbations as p300 KIX (data not shown). Quantification of chemical shift perturbations at the 1:1 molar ratio for p300 KIX and CRY1 CC are depicted in Figure 4a and b, respectively.

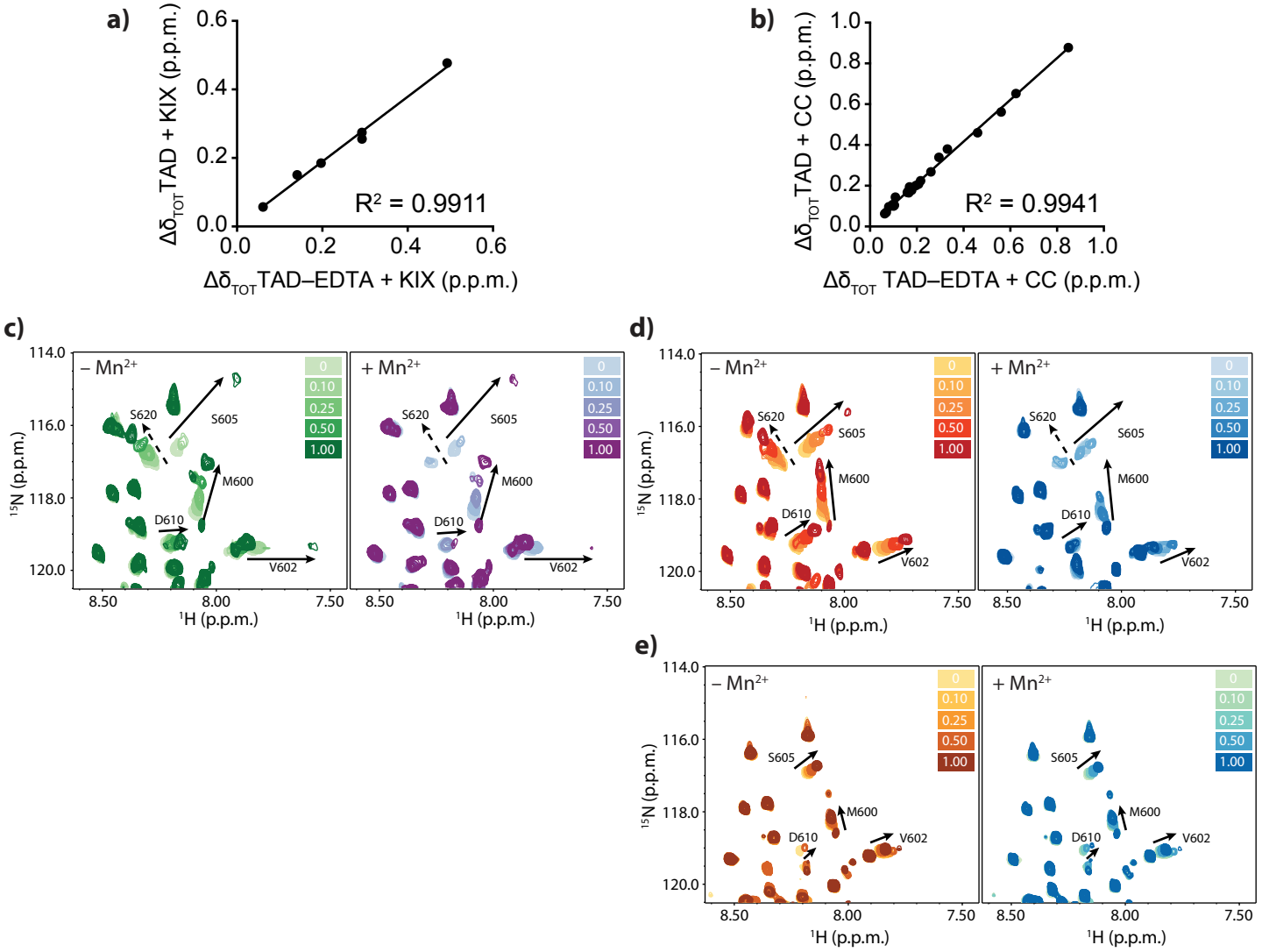

Supplementary Figure 5. The TAD undergoes dynamic structural rearrangement upon binding to the p300 KIX domain and CRY1 CC peptide to couple the TAD helix and C-terminus. **(a-b)** Covalent coupling of the MTS-EDTA moiety at a C-terminal cysteine (TAD–EDTA) does not perturb interactions with p300 KIX or CRY1 CC. Correlation of chemical shift perturbations in WT TAD or TAD-EDTA ^{15}N BMAL1 TAD upon complex formation at 1:1 stoichiometry with p300 KIX domain **(a)** or CRY1 CC peptide **(b)**. Each point represents the chemical shift perturbation of a different backbone amide. Goodness-of-fit for linear regression (R^2) is shown for both correlations. **(c-d)** ^{15}N HSQC spectra of ^{15}N TAD–EDTA ±Mn^{2+} titrated with p300 KIX **(c)** or CRY1 CC **(d)** up to 1:1 stoichiometry. Inset legends represent various steps of relative stoichiometry of p300 KIX or CRY CC to ^{15}N BMAL1 TAD–EDTA in the absence (left panel) or presence (right panel) of chelated Mn^{2+}. Arrow lengths and orientation are maintained within all panels to illustrate changes (or lack thereof) in chemical shift perturbation upon chelation of paramagnetic Mn^{2+}. Dashed arrow for residue Ser620 illustrates a residue in the TAD C-terminus that undergoes complex-independent broadening due to its proximity to the C-terminal PRE label (see Figure 4d). **(e)** ^{15}N HSQC spectra of ^{15}N TAD 619X–EDTA ±Mn^{2+} titrated with CRY1 CC peptide demonstrate the lack of CRY1-dependent broadening at the TAD helix in the absence of the C-terminal seven residues.

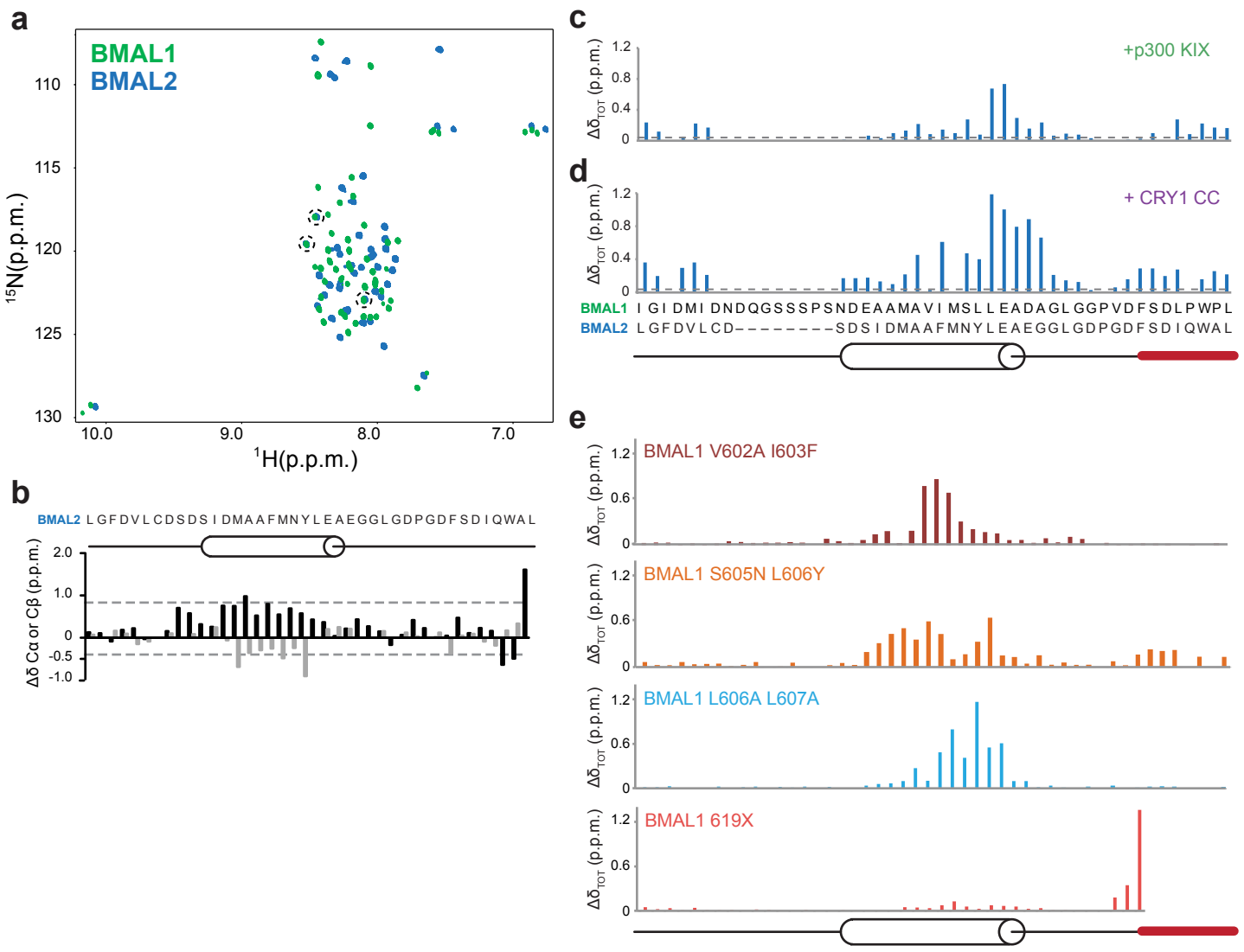

Supplementary Figure 6. Comparison of BMAL1 and BMAL2 TAD domains by NMR spectroscopy. **(a)** ^{15}N HSQC spectra of ^{15}N BMAL1 TAD (green) or ^{15}N BMAL2 TAD (blue) demonstrate minimal overlap of chemical shifts. Dashed circles indicate the only residues that have similar chemical shifts; these residues represent the conserved N-terminal vector artifact left after TEV cleavage. **(b)** The BMAL2 TAD has a modest propensity for α-helix formation, demonstrated by comparison of Cα (black) or Cβ (gray) chemical shifts to the chemical shift index of random coil shifts (Δδ)[31,32]. Dashed line: significance cutoff for helical prediction from Δδ analysis. **(c-d)** Comparison of BMAL TAD interactions with the CBP(p300) KIX domain and CRY1 CC peptide. Chemical shift changes ($\Delta\delta_{TOT}$) on ^{15}N BMAL2 TAD for the 1:1 molar ratio of either CBP(p300) KIX domain **(c)** or the CRY1 CC peptide **(d)**. Dashed line: significance cutoff of 0.04 p.p.m. for chemical shift perturbations. The BMAL TAD sequences are aligned underneath NMR data with predicted secondary structure: barrel, predicted α-helix; red line, C-terminal seven residues; black line, no predicted structure. **(e)** Mutations in BMAL1 TAD induce local chemical shift perturbations. Bar graphs plot total chemical shift perturbation ($\Delta\delta_{TOT}$) of backbone shifts from ^{15}N HSQC spectra of mutant TADs compared to WT TAD. Mutations in the α-helix largely perturb just the helix and truncation of the C-terminal seven residues gives rise to large chemical shift perturbations only at the new C-terminus.

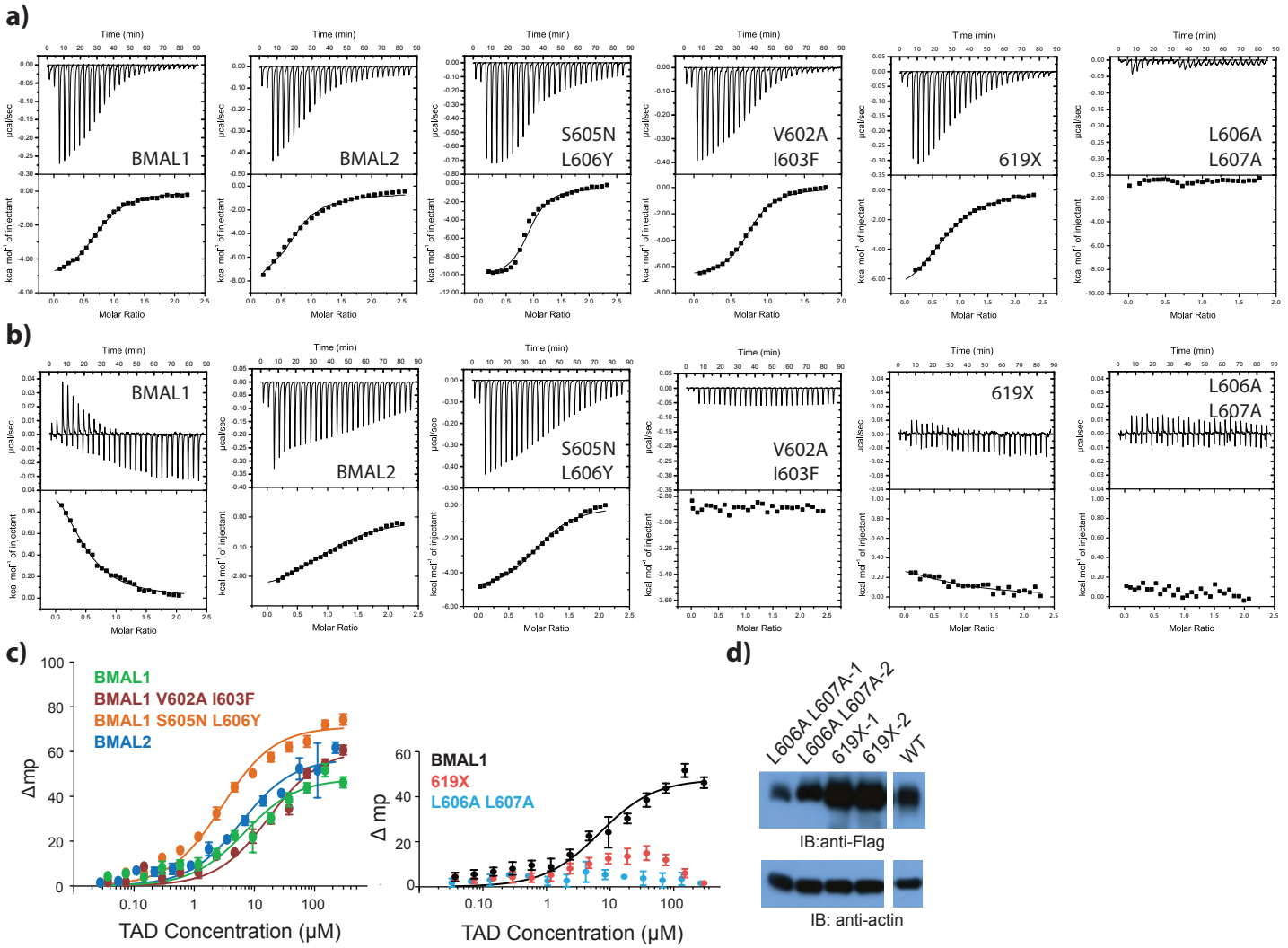

Supplementary Figure 7. Quantitative analysis of BMAL TAD interactions with transcriptional coregulators. **(a-b)** Data from isothermal titration calorimetry (ITC) experiments of BMAL TAD (BMAL1, BMAL2, or BMAL1 mutants, as indicated above) with either CBP KIX domain **(a)** or the CRY1 CC peptide **(b)**. All ITC experiments were set up with 15-30 μM TAD in the cell and 220-250 μM KIX or CRY1 CC peptide in the syringe (details for each experiment can be found in Online Methods) and run at 25°C. Data shown are representative of at least two independent ITC runs. ITC data were fit to a one-site binding model (Origin) to derive parameters that populate Table 1, with representative *N* values of 0.7-1.0 to indicate 1:1 stoichiometry. **(c)** Fluorescence polarization-based titration of rhodamine-labeled CRY1 CC peptide against BMAL1, BMAL2 or BMAL1 mutant TADs. Data are shown as mean change in milli-polarization units (Δmp) from free CC peptide ± s.d. error bars from four replicates in a representative experiment ($n = 3$ independent experiments). Curves were fit by non-linear regression to a one-site binding model (GraphPad Prism) to determine K_D values in Table 1. **(d)** Relative protein expression of BMAL1 WT and mutant constructs within the complemented *Bmal1*$^{-/-}$ *Per2*^{Luc} lines were determined by western blot using indicated antibodies.

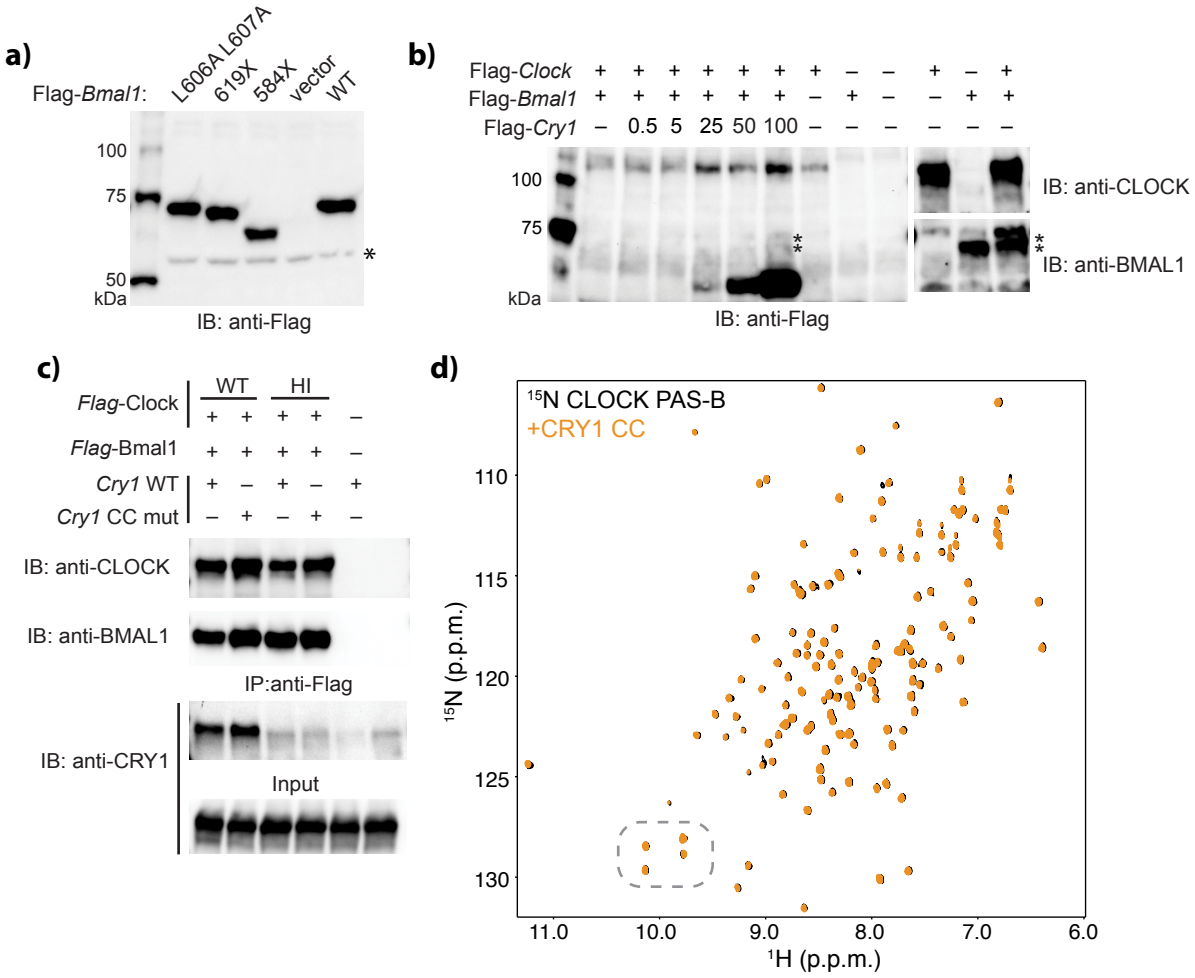

Supplementary Figure 8 CRY1 regulation of CLOCK–BMAL1 requires interaction with both CLOCK and BMAL1. **(a)** Wild-type and mutant Flag-*Bmal1* clones are expressed to similar levels in HEK293T cells as determined by western blot using anti-Flag antibody. *, non-specific band that serves as a loading control. **(b)** Relative expression levels of CLOCK, BMAL1 and CRY1 with plasmid ratios used in luciferase assays. HEK293T cells were transfected with plasmid ratios used in *Per1*-luciferase assay (100 ng each *Clock* and *Bmal1*, and *Cry1* plasmid as indicated, scaled 4X for increase in culture dish area). Relative protein expression levels are shown by western blotting using indicated antibodies. Under these experimental conditions, BMAL1 expression is just at the detection limit with the anti-Flag antibody. Expression of CLOCK and BMAL1 was also verified by blotting with anti-CLOCK and anti-BMAL1 antibodies, which provide greater sensitivity of detection compared to the Flag antibody. **, migration of the CLOCK-dependent phosphorylated BMAL1 species in the anti-Flag blot relative to its detection with the anti-BMAL1 antibody. **(c)** Mutation of the CLOCK PAS-B HI loop (Q361P W362R) disrupts interaction with CRY1 by anti-Flag co-IP when co-expressed with Flag-BMAL1 in HEK293T cells. The CRY1 CC mut (R501Q K503R)[66] does not affect interaction of CRY1 with co-expressed Flag-CLOCK and Flag-BMAL1. **(d)** The CRY1 CC helix does not bind directly to the CLOCK PAS-B domain. ^{15}N HSQC spectra of 60 μM ^{15}N CLOCK PAS-B in the absence (black) and presence (orange) of 240 μM CRY1 CC peptide show no chemical shift perturbations upon addition of CRY1 C peptide. Dashed box: tryptophan indole region shown in Figure 6g. Assignment of the CLOCK PAS-B W362 tryptophan indole peak was made by mutagenesis (data not shown).